Reactive Uptake of Nitric Acid into Aqueous Sodium Chloride Droplets Using Real-Time Single-Particle Mass Spectrometry

Michael P. Tolocka, Thomas D. Saul, and Murray V. Johnston*

Department of Chemistry and Biochemistry, University of Delaware, Newark, Delaware 19716

Received: September 2, 2003; In Final Form: February 5, 2004

The kinetics and rate-limiting mechanism of reactive uptake of nitric acid into submicron, deliquescent sodium chloride aerosols are determined. The reaction was performed in a flow tube with a real-time single-particle mass spectrometer connected to the outlet to determine the chloride-to-nitrate ratio of the transformed particles. Pseudo-first-order conditions were maintained by keeping the nitric acid pressure constant, as measured with a chemiluminescence analyzer. Experiments were performed with 100−220 nm diameter droplets at ca. 80% relative humidity and nitric acid concentrations between 60 and 380 ppb. Rate constants and uptake coefficients were determined from time-dependent changes in the chloride concentration of individual particles that traversed the reactor. The initial reactive uptake coefficient for 100 nm droplets was found to be $4.9 \pm 2.7 \times 10^{-3}$ and, to a first approximation, independent of the nitric acid concentration. The uptake coefficient also was found to increase linearly with increasing droplet size over the size range studied. These dependencies suggest that transport phenomena (diffusion of $HNO_{3(g)}$ to the droplet surface, accommodation of HNO_3 into the droplet, diffusion of $HNO_{3(aq)}$ and $HCl_{(aq)}$ inside the droplet, and transport of HCl across the droplet surface into the gas phase) do not limit the reaction rate. Instead, reactive uptake of $HNO_{3(g)}$ is limited by formation of molecular HCl in the aqueous phase—a thermodynamically controlled process. The results are consistent with related measurements that show uniform chloride/nitrate/sodium mole ratios in submicron-size aerosols, a large uptake coefficient for aerosols in the low micron-size range, and decreasing chloride-to-nitrate ratios (because of transport limitations) in supermicron-size aerosols.

Introduction

Sea-salt is the second largest component by mass of the atmospheric aerosol global burden, a smaller load than mineral dusts but greater than sulfates, products of biomass burning, and secondary organics.[1] In the marine boundary layer, sea-salt aerosols are produced by breaking waves and bursting bubbles on the ocean surface. Particulate salts exist as concentrated aqueous droplets above their deliquescence point, a common occurrence in the marine environment. These droplet sizes range from less than 100 nm to about 10 μm in diameter. The reactions of sea-salt particles with gas-phase species have garnered interest because of their importance in the cycling of halogens in the atmosphere.[2] For example, acid-displacement has been proposed to explain the depletion of chloride and enrichment of nitrate in marine boundary layer aerosols:

$$NaCl + HNO_{3(g)} \rightarrow NaNO_3 + HCl_{(g)} \qquad (1)$$

The nitrate salt produced by reaction 1 will eventually return to the ground by precipitation (e.g., rainfall), contributing to nitrogen saturation in the coastal ecosystem.[3] It may also substantially influence the radiative properties of the marine boundary layer. Murphy et al.[4] have found that almost all fine particles above 0.13 μm in diameter at a remote southern ocean region contain sea-salt. Aerosols in this size range efficiently scatter solar radiation and act as condensation nuclei. Coarse sea-salt particles facilitate the removal of airborne pollutants by counteracting the precipitation suppression effect of the large numbers of fine particles produced by anthropogenic activities.[5] Sea-salt aerosols also serve as vehicles for transport and reaction of organic components.[6] For example, Middlebrook et al.[7] observed organic components in over half the particles that contain sea-salt in clean air and more than 60% during pollution events. The influence of acid displacement on these processes is likely to be greatest where marine air interacts with polluted environments, such as the southern California coastline, the Gulf coast region, and the eastern seaboard of the United States.

In the atmosphere, reaction 1 can proceed on solid particles or in concentrated droplets, depending on whether the relative humidity is below or above the efflorescence/deliquescence points. In the laboratory, this reaction has been studied on powders[8] and crystals[9] in Knudsen cells, on pressed powders[10,11] and airborne particles[12−14] in flow tubes, and on single crystals in ultrahigh vacuum.[15] The reactive uptake coefficient (γ), defined as the fraction of HNO_3 collisions with the surface that result in a reaction, varies by more than 2 orders of magnitude (10^{-4}−10^{-2} range) in experiments with nominally "dry" solids. This variation arises from strong dependencies on the residual water content of the sodium chloride surface[8,10,15,16] and the HNO_3 pressure.[10,11] Experiments performed with liquid droplets above the deliquescence and/or efflorescence relative humidities give much higher values for γ, 0.2 or greater.[13,14]

In the work described here, a new detection approach is used to study reaction 1; it facilitates experimentation above the deliquescence relative humidity for submicron droplet sizes, where the changes in the marine aerosol chemical composition can strongly influence light scattering. In addition, the reaction is performed under constant HNO_3 pressure to facilitate

* Author to whom correspondence should be addressed. Telephone: 302-831-8014. Fax: 302-831-6335. E-mail: mvj@udel.edu.

10.1021/jp036612y CCC: $27.50
Published on Web 03/12/2004

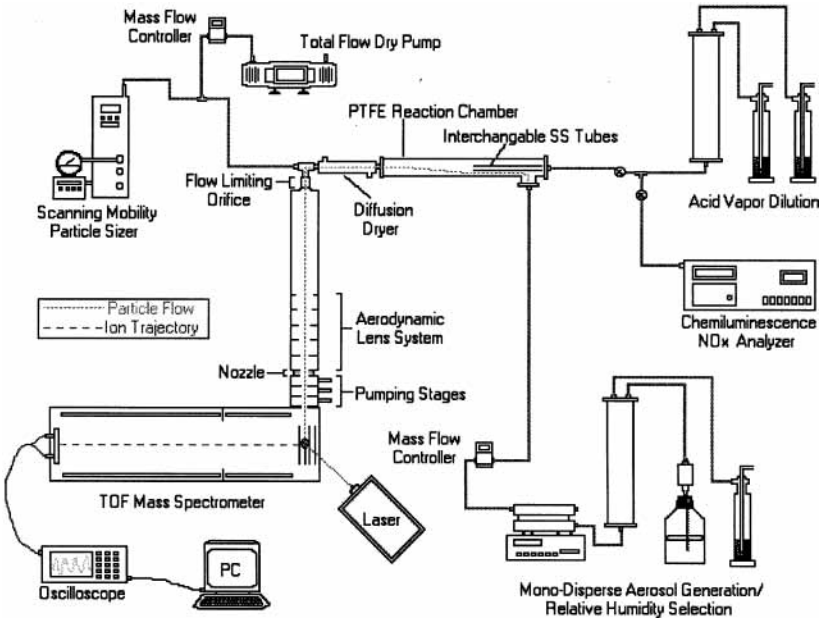

Figure 1. Experimental setup.

investigation of the pressure dependence. The detection approach is based upon real-time single-particle mass spectrometry.[17,18] This method has been used for over a decade to characterize individual particles, including those undergoing chemical reaction.[19,20] Semiquantitative measurements of particle composition are also possible in some instances.[21−24] For reaction 1, single-particle mass spectrometry provides the opportunity to monitor changes in the particle phase composition as a function of contact time with HNO_3 vapor.

Experimental Section

The experimental apparatus to study reactive uptake is shown in Figure 1. The main components are a flow tube reactor, a chemiluminescent nitrogen oxide analyzer to monitor the HNO_3 partial pressure,[25,26] and a real-time single-particle mass spectrometer to monitor the condensed-phase composition.

The flow tube reactor is constructed from a 2.54/2.22 cm o.d./i.d. 125 cm long Teflon-coated stainless steel tube. The (laminar) flow velocity in the tube is 4 cm/s, corresponding to a total residence time of 31 s. The length of the central injection tube determines the contact time between the reactants. The flow tube pressure is maintained near atmospheric pressure (760 Torr) and is measured with a capacitance manometer (Pfeiffer Vacuum, CMR271, Nashua, NH). Particle losses to the walls are insignificant, as expected from previous results.[27−32]

A polydisperse aerosol is produced using a constant output generator (model 3076, TSI, Inc., St. Paul, MN) to atomize a 0.1 g/L solution of sodium chloride in deionized (18 MΩ) water from a Millipore Simplicity 185. The relative humidity of the aerosol is regulated by dilution air that passes through bubblers containing pure water. In these experiments, the relative humidity in the flow reactor is set to 80% as measured with a NIST-traceable hygrometer (model 11-661-7B, Fisher Scientific, Pittsburgh, PA). Because the relative humidity is above the deliquescence point, the sodium chloride particles exist as liquid droplets with an approximate concentration of 5 M.[33] The droplet size (100−250 nm diameter) is selected with a home-built radial mobility analyzer.[34] The aerosol size distribution is measured with a scanning mobility particle-sizing instrument (model 3936, TSI, Inc., St. Paul, MN). In all cases the distribution is nearly monodisperse, $\sigma_g < 1.2$ for a single charge state, and the ratio of singly to doubly charged particles is typically 5:1 (number density). All kinetic calculations are based upon the combined size distribution of singly and doubly charged particles. The particle number concentration varies by less than ±5% throughout an experiment.

Nitric acid vapor is generated by bubbling compressed air through a solution of concentrated (15.8 M) HNO_3. The resulting air stream is diluted using humidified air. A chemiluminescence analyzer (Thermo Environmental model 43, Franklin, MA) measures the HNO_3 partial pressure entering and exiting the flow tube reactor. The HNO_3 pressures in the reactor are within ±10% of the predictions based on Henry's Law and dilution factors. Measurements of the HNO_3 pressure before and after the flow tube reactor confirm that it remains constant under the conditions used in the experiment and that wall losses are minimal.

The real-time single-particle mass spectrometer has been described in detail elsewhere.[35] The aerosol is sampled through an inlet at 150 cm^3/min. The inlet contains an aerodynamic lens system[36] to focus particles into a collimated beam. The particle beam passes through three differential pumping stages before entering the ion source region of a linear time-of-flight mass analyzer that is operated in the negative ion mode.[37] As shown below, negative ion detection permits simultaneous detection and quantification of chloride and nitrate in a single particle. The particle beam intercepts an excimer laser beam (193 nm, 3−8 mJ/pulse, 10 ns pulse width). The laser fires continuously at 20 Hz. If a particle is coincident with the laser pulse, then it is ablated and ionized. The particle is considered "detected" and a mass spectrum is recorded if the ion current exceeds a threshold value (50 mV) within a set time window that corresponds to $15 < m/z < 50$. This threshold value is set to the lowest signal level such that no spectra are recorded in the absence of particles. While particles in the flow tube reactor exist in the form of liquid droplets, dry particles must be analyzed by the mass spectrometer to eliminate measurement artifacts.[22,38−40] This is accomplished by passing the droplets through a Nafion diffusion drier (Perma Pure, MD-110, Toms River, NJ) prior to entering the mass spectrometer. The residence

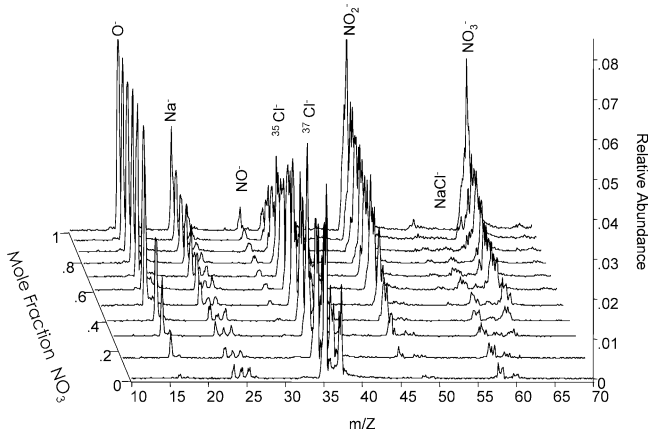

Figure 2. Mass spectra of NaCl/$NaNO_3$ particles generated from standard solutions.

time in the drier is ca. 300 ms. The ratio of the wet droplet diameters to the dry particle diameters are within experimental error of the 5 M concentration of NaCl in the droplets expected from thermodynamics.[33]

To quantify the relative amounts of chloride and nitrate in the droplets, standard solutions of NaCl/$NaNO_3$ are atomized and analyzed. Figure 2 shows the negative ion spectra of standard particles containing different relative amounts of NaCl and $NaNO_3$. Each spectrum is the average of 100 single-particle spectra. Prominent peaks in the spectra of pure NaCl particles include Na^- (or possibly NO_2^{2-}, $m/z = 23$), Cl^- ($m/z = 35$ and 37), and $NaCl^-$ ($m/z = 58$). As the $NaNO_3$ content increases, peaks corresponding to O^- ($m/z = 16$), NO^- ($m/z = 30$), NO_2^- ($m/z = 46$), and NO_3^- ($m/z = 62$) grow in intensity. A relative ion response (RIR) is obtained from the integrated signal corresponding to the chloride present in the droplet ($S_{Cl,}$ sum of signals at $m/z = 35$ and 37) divided by the signal corresponding to the chloride plus nitrate present in the droplet ($S_{NO_x} + S_{Cl}$, sum of signals at $m/z = 35$, 37, 46, and 62):

$$\mathrm{RIR} = \left(\frac{S_{\mathrm{Cl}}}{S_{\mathrm{NO_x}} + S_{\mathrm{Cl}}}\right) \tag{2}$$

The RIR is related to the mole fraction of chloride in the particle by a third-order polynomial fit:

$$X_{\mathrm{Cl}} = A(\mathrm{RIR})^3 + B(\mathrm{RIR})^2 + C(\mathrm{RIR}) + D \tag{3}$$

where A, B, C, and D are constants. For each mole fraction, the mean RIR is obtained by averaging the RIRs from three separate experiments, 100 single-particle spectra each. The results, shown in Figure 3, include repeat measurements made over a several month period, illustrating the robustness of the calibration. The nonlinear relationship between mole fraction and RIR in Figure 3 indicates that the relative response factors for chloride and nitrate are different. Fitting the plot in Figure 3 to a standard ion response function[22] gives a relative response of 0.48 for chloride to nitrate. While the standard ion response function does fit the data, the third-order polynomial provides greater precision and accuracy for subsequent calculations. The plot in Figure 3 is invariant with particle size over the range of sizes included in this study.

Results

In this experiment, individual particles are analyzed. Although chemical composition measurements are averaged over 100 particles to improve precision, each individual measurement is

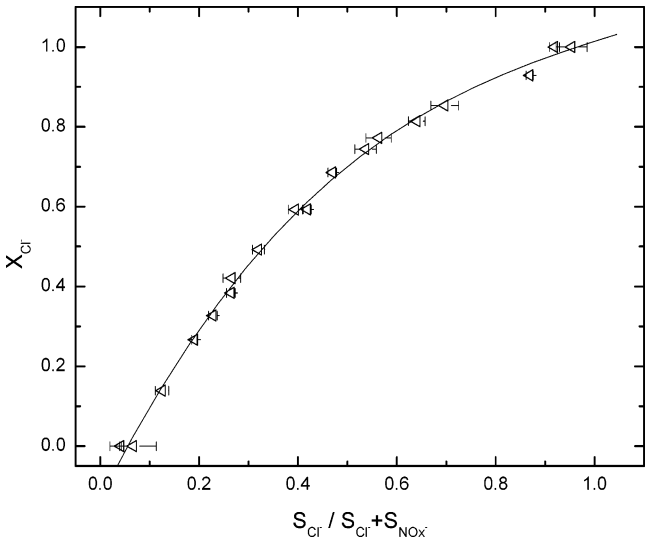

Figure 3. Relative ion response plotted versus the mole fraction of chloride. Error bars indicate one standard deviation.

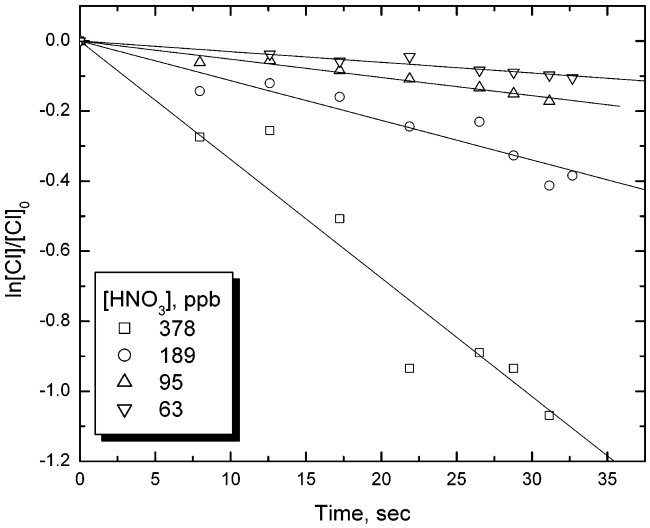

Figure 4. Loss of chloride ion concentration versus time. Each data set is fit to a first-order exponential decay to determine the rate coefficient.

the result of a single droplet interacting with HNO_3 vapor as it moves through the flow tube reactor. Accordingly, the average chloride concentration in a single droplet emerging from the flow tube can be calculated from the mole fraction (X_{Cl}) as determined from eq 3 and Figure 3:

$$[\mathrm{Cl}^-] = \frac{d_{\mathrm{p}}^3 \rho_{\mathrm{p}} X_{\mathrm{Cl}}}{d_{\mathrm{d}}^3 W_{\mathrm{NaCl}}} \tag{4}$$

where d_p is the dry particle diameter before exposure to HNO_3, ρ_p is the density of sodium chloride, d_d is the (wet) droplet diameter before exposure to HNO_3, and W_{NaCl} is the formula weight of sodium chloride. The chloride concentration remaining in the droplet is then plotted versus contact time in the flow tube reactor. Figure 4 shows chloride concentration vs time plots for 100 nm diameter droplets. Because the HNO_3 pressure remains constant during the reaction, these plots can be fit to first-order exponential curves to obtain the pseudo-first-order rate constant at each HNO_3 pressure.[41−44] Figure 5 shows that the pseudo-first-order rate constant (k_I) increases with increasing HNO_3 concentration, as expected. For the discussion below, the

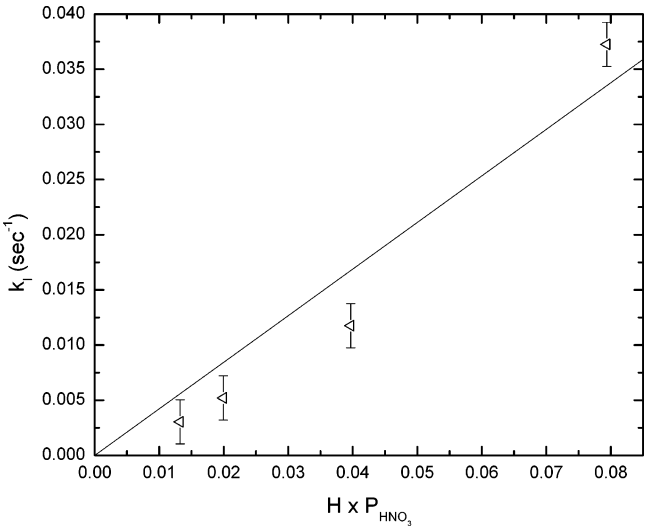

Figure 5. The first-order rate coefficient vs droplet concentration of HNO_3. Line is an error-weighted fit to the data ($R^2 = 0.95$).

TABLE 1: Experimentally Determined Pseudo-First-Order Rate Constants and Initial Uptake Coefficients

$[HNO_3]$, ppb	k_I ($\times 10^{-2}$)	γ_o ($\times 10^{-3}$)
378	-3.73 ± 0.19	6.9 ± 4.1
189	-1.18 ± 0.07	4.4 ± 2.6
95	-0.520 ± 0.028	3.9 ± 2.3
63	-0.304 ± 0.011	4.5 ± 2.7
average		4.9 ± 2.9

dependence in Figure 5 is assumed to be linear. This assumption is revisited at the end of the paper.

For a series of single-particle measurements at a given HNO_3 pressure, the time-dependent loss rate of chloride ions in a droplet (mol L^{-1} s^{-1}) is given by

$$-\frac{\partial[Cl^-]}{\partial t} = k_I[Cl^-] = k_{II}HP_{HNO_3}[Cl^-] \qquad (5)$$

where k_I is the pseudo-first-order rate constant obtained from the plot in Figure 4, $[Cl^-]$ is the chloride concentration remaining in the droplet at the particular time, k_{II} is the second-order rate constant, H is the Henry's Law constant, and P_{HNO_3} is the (constant) partial pressure of nitric acid vapor. The reactive uptake coefficient (γ) is given by

$$\gamma = -\frac{\partial[Cl^-]}{\partial t}\frac{2d_d}{3u[HNO_3]} \qquad (6)$$

where the reaction rate is normalized by the collision rate of HNO_3 with an individual particle. In this equation d_d is the droplet diameter, u is the average molecular speed of nitric acid, and $[HNO_3]$ is the gas-phase concentration. These equations assume first-order kinetic gain to the particle; that is, the observation of nitrate in the particle is coincident with loss of chloride.

Equations 5 and 6 show that the reactive uptake coefficient is a maximum at the beginning of the reaction and decreases as chloride is converted to nitrate. The initial uptake coefficient ($\gamma_{o,net}$) is obtained by substituting the initial chloride concentration into eq 5. The results are shown in Table 1 for 100 nm diameter droplets. The initial reactive uptake coefficient is approximately 5×10^{-3}, independent of HNO_3 concentration over the range studied. Inspection of eqs 5 and 6 shows the reason for this independence: both the numerator and the denominator of eq 6 increase linearly with HNO_3 pressure. This result is consistent with the prediction by Ghosal and Hemminger.[15]

In principle, several processes could affect the measured value of γ_o. First, HNO_3 could be incorporated into the droplet without displacement of HCl vapor. Based on the Henry's Law constant for HNO_3,[45] the maximum concentration of HNO_3 in the droplet is 0.08 M, which is only ca. 2% of the initial sodium chloride concentration at 80% RH (ca. 5 M). This dissolved nitric acid is likely to be removed during the particle drying step. Drying should result in expulsion of an equivalent amount of $HCl_{(g)}$, causing an apparent increase in the chloride-to-nitrate ratio in the droplet. Since the initial sodium chloride concentration is large, any changes due to this phenomenon during drying are small and within the measurement uncertainty. Second, our calculations for the corrections associated with longitudinal pressure drop and axial diffusion suggest they are unimportant.[46] Third, modification of measured uptake coefficients due to radial diffusion must be considered. Following previous approaches,[10,13] the calculated uptake coefficients change by $<10\%$, assuming a diffusion coefficient of HNO_3 in air of 0.135 cm^2/s.[13]

While the precision of the k_I measurement is quite good ($\pm 5\%$ rsd), the uncertainty of γ_o is much larger because of the bimodal particle size distribution (singly and doubly charged particles) for both d_d (the droplet diameter) and d_p (the dried particle diameter). Other factors in the γ_o determination include uncertainties in the nitric acid concentration, flow calibrations, and chemical composition measurement by single-particle mass spectrometry. Together these factors give overall uncertainties on the order of 40−60% rsd. The accuracy of the γ_o measurement would be most strongly influenced by systematic error in the nitric acid concentration.

Discussion

Reactive uptake is often viewed in the context of a resistive model,[41,42,47−51] where the net uptake (γ_{net}) is approximated by a series of steps that include diffusion of the gas-phase reactant to the droplet surface (Γ_g), accommodation of the gas-phase reactant on the droplet surface (α), reaction inside the droplet (Γ_{rxn}), and solubility/diffusion of the gas-phase reactant inside the droplet (Γ_{sol}):

$$\frac{1}{\gamma_{net}} = \frac{1}{\Gamma_G} + \frac{1}{\alpha} + \frac{1}{\Gamma_{rxn} + \Gamma_{sol}} \qquad (7)$$

The gas-phase diffusion term Γ_G is given by the rate of diffusion to the droplet surface normalized by the collision rate:

$$\Gamma_G = \frac{Kn(1 + Kn)}{0.75 + 0.283Kn} \qquad (8)$$

where

$$Kn = \frac{6D_g}{ud_d} \qquad (9)$$

and D_g is the gas-phase diffusion coefficient. For diffusion of HNO_3 molecules to a 100 nm diameter NaCl droplet, $1/\Gamma_G = 0.37$, which is much less than 1% of the net uptake if $\gamma_{net} = 5 \times 10^{-3}$. In fact, this is an advantage of studying small-diameter particles: uptake is not significantly limited by $HNO_{3(g)}$ transport to the droplet surface.

The accommodation or sticking coefficient (α) is the probability that a gas-phase reactant molecule striking the droplet surface crosses the interface into the condensed phase. Typical

values for α are on the order of 0.1 or greater,[52,53] which indicates that uptake is not significantly limited by accommodation of $HNO_{3(g)}$ on the surface.

If it is assumed that the $HNO_{3(aq)}$ is initially in Henry's law equilibrium only at the droplet surface and then diffuses into the bulk until equilibrium is achieved, Γ_{sol} can be written:

$$\Gamma_{sol} = \frac{4HRT}{u}\sqrt{\frac{D_l}{\pi t}} \qquad (10)$$

where t is the contact time between the gas-phase reactant and droplet. At $t = 0$, $1/\Gamma_{sol}$ is zero and therefore does not contribute significantly to γ. As time increases, $1/\Gamma_{sol}$ also increases. For the reaction studied here, $1/\Gamma_{sol} = 4$ at 31 s, which is still insignificant relative to $1/\gamma_{net}$ at this time. (Note that γ_{net} decreases with increasing reaction time.)

The above discussion suggests that Γ_G, α, and Γ_{sol} do not contribute substantially to the observed reactive uptake coefficient. The main contribution to γ_{net} is then given by the Γ_{rxn}. Recently, Baer[54] and Worsnop[55] have derived reaction rate expressions for specific physical mechanisms of reactive uptake. Table 2 gives adaptations of these expressions for the reaction in eq 1. A logarithmic dependence of concentration vs time (integral of eq 5) applies, for example, when the rate is limited by reaction at the droplet surface, reaction in the bulk of the droplet (where the diffuso-reactive length is larger than the droplet radius), or condensed-phase diffusion. A logarithmic dependence does not apply when the rate of uptake is limited by gas-phase diffusion or reaction in the bulk where the diffuso-reactive length is smaller than the droplet radius.

Which of the mechanisms in Table 2 limits reactive uptake? The gas-phase and condensed-phase diffusion mechanisms are inconsistent with the 100 nm diameter droplet data. Gas-phase diffusion is inconsistent with a logarithmic dependence of concentration vs time (see Figure 4 and Table 2), while condensed-phase diffusion is inconsistent with Figure 6, which shows a linear relationship between $\ln[Cl]/[Cl]_0$ vs exposure ($P_{HNO_3} \times t$).

Distinguishing the remaining mechanisms requires knowledge of how uptake depends on droplet size. The droplet-size dependence was studied with a sufficiently high precision by keeping the reaction time and nitric acid concentrations constant and switching back and forth very quickly between two sizes. Pseudo-first-order conditions were maintained as before. Figure 7 shows the results of one such experiment in which the droplet size was switched between 100 and 175 nm diameter while keeping the reaction time (15.5 s) and nitric acid concentration (300 ppb) constant. Within experimental error, the mole fraction of chloride remaining at the end of the reaction period is equal for the two sizes. The lack of a droplet-size dependence is consistent with the reaction in the particle ($l > r$) mechanism but not with the surface or reaction in the particle ($l < r$) mechanisms. The latter two mechanisms require that the mole fraction of chloride remaining in the droplet *increase* with increasing particle size. The expected increase for these mechanisms and the conditions in Figure 7 (from a mole fraction of 0.55 at 100 nm to 0.71 at 175 nm) would have been easily detected within the precision of the measurement if these mechanisms had limited uptake.

Additional experiments with other combinations of droplet sizes between 100 and 250 nm and with other reaction times gave the same result—the mole fraction of chloride remaining in the droplet is independent of droplet size. Because of limitations in the experimental setup, droplet sizes outside these

TABLE 2: Concentration and Uptake Expressions for Different Mechanisms that Limit Uptake[a]

	Mechanism of Uptake			
	surface reaction	reaction in particle ($l < r$)	reaction in particle ($l > r$)	condensed-phase diffusion	gas-phase diffusion[b]
concentration	$\ln\frac{[Cl]}{[Cl]_o} = -\frac{3\delta^2}{r}HP_{HNO_3}k_{II}^{surf}t$	$\frac{\sqrt{[Cl]}}{[Cl]_o} = 1 - \frac{3HP_{HNO_3}\sqrt{D_l k_{II}}}{2r}t$	$\ln\frac{[Cl]}{[Cl]_o} = -HP_{HNO_3}k_{II}t$	$\ln\frac{[Cl]}{[Cl]_o} = -\frac{12D_l}{r^2}t$	$\frac{[Cl]}{[Cl]_o} = 1 - \frac{3ng_u}{4[Cl^-]_o r}\left(\frac{1}{\Gamma_{diff}} + \frac{1}{\alpha}\right)^{-1}t$
uptake	$\Gamma_{rxn} = \frac{4HRT}{u}\delta^2 k_{II}^{surf}[Cl]_o$	$\Gamma_{rxn} = \frac{4HRT}{u}\sqrt{D_l k_{II}[Cl]_o}$	$\Gamma_{rxn} = \frac{4HRT}{3u}k_{II}[Cl]_o$	$\Gamma_{obs} = \frac{8D_l[Cl^-]_o}{n_g r u}\sum_1^\infty e^{(-iD_l g^2 t/r^4)}$	$\Gamma_{obs} = \frac{Kn}{0.75 + 0.283Kn}$

[a] $[Cl^-]$ is the chloride concentration in the droplet, H is the Henry's Law coefficient of nitric acid, R is the gas constant, T is temperature, n_g is the gas-phase number concentration of nitric acid molecules available to react, D_l is the diffusion coefficient of the reactants in the droplet, r is the droplet radius, u is the average molecular speed of nitric acid vapor, K_S is an equilibrium constant used to determine how many molecules are available for surface reaction, k_{II} is the second-order rate coefficient, and t is time. [b] Or could be limited by mass accommodation.

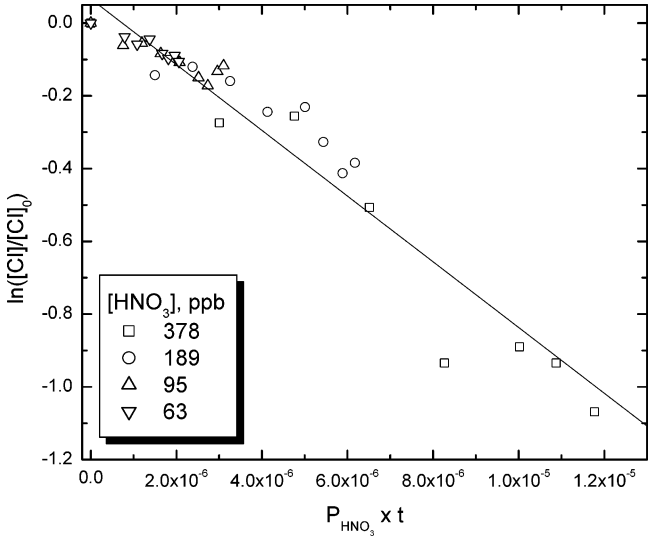

Figure 6. Chloride ion loss as a function of $HNO_{3(g)}$ exposure.

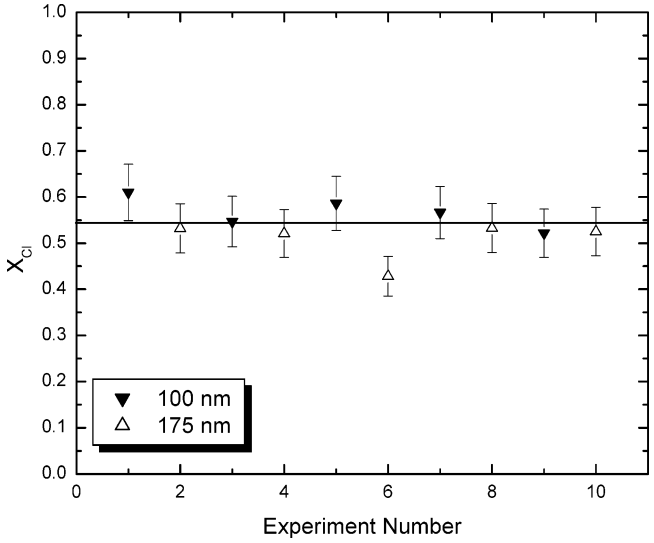

Figure 7. Sequential measurements of X_{Cl} by switching back and forth between 100 and 175 nm droplets. The time required to complete each measurement and switch to the next droplet size was 20 min.

bounds could not be studied. However, the results are consistent with those of ten Brink[12] who found in a smog chamber experiment that the chloride/nitrate/sodium mole ratios remained constant for droplet sizes between 0.6 μm and 2.2 μm in diameter.

Taken together, these results suggest that *reactive* uptake of HNO_3 is limited by formation of HCl in the condensed phase. Nitric acid uptake can be thought of as a two-step process.[12] Initially, HNO_3 rapidly enters the droplet as it equilibrates between the gas and droplet phases, acidifying the droplet. This process occurs much faster than the time scale of our measurements. Indeed, calculations suggest a τ_{max} of 4 s [56] (or perhaps less, ca. 0.4 s[57]) for establishing equilibrium across the gas−liquid interface. Once equilibrium is established, further (reactive) uptake of $HNO_{3(g)}$ requires displacement of an equal amount of $HCl_{(g)}$. This second step is much slower. The results presented above show that diffusion of $HNO_{3(g)}$ to the droplet surface, accommodation of HNO_3 into the droplet, and diffusion of $HNO_{3(aq)}$ and $HCl_{(aq)}$ inside the droplet do not limit the reaction rate. Also, it is highly unlikely that transport of HCl across the droplet surface into the gas phase is limiting.[58] Therefore, the reaction rate, and hence further uptake of $HNO_{3(g)}$,

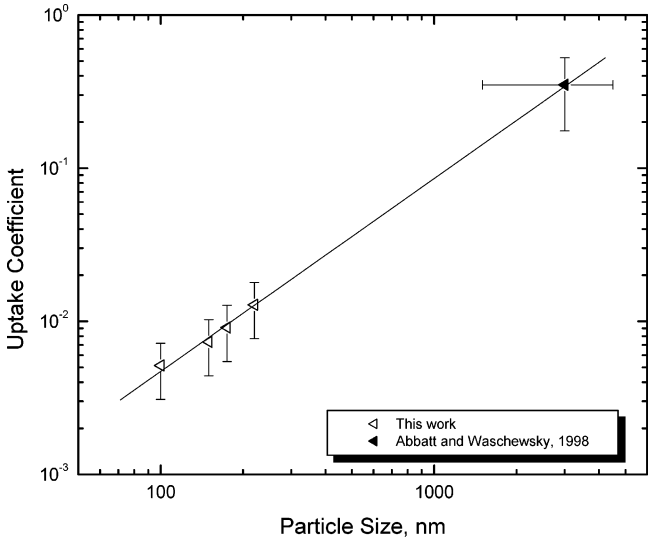

Figure 8. Uptake coefficient ($\gamma_{o,net}$) versus droplet size for this work and Abbatt and Waschewsky.[13] Error bars for this work indicate the propogation of error for γ_o calculation. (As explained in the text, the reaction rates are determined with much higher precision.) For the referenced work, *Y*-error bars designate uncertainty in the measurement, while *X*-error bars indicate the particle size distribution.

is apparently limited by formation of $HCl_{(aq)}$:

$$H^+_{(aq)} + Cl^-_{(aq)} \rightleftharpoons HCl_{(aq)} \qquad (11)$$

At equilibrium, the reaction in eq 11 lies far to the left as the pK_a of $HCl_{(aq)}$ is approximately −6.[59] If one assumes equilibrium concentrations of ions in the droplet based upon Henry's Law for HNO_3 and the solubility of NaCl at 80% RH, then the Henderson−Hasselbalch equation predicts an initial concentration on the order of 1 molecule of $HCl_{(aq)}$ in a 100 nm diameter droplet. The rate of $HCl_{(g)}$ release into the gas phase is low because there are few $HCl_{(aq)}$ molecules available to be displaced.

If the number of $HCl_{(g)}$ molecules released into the gas phase is determined by the number of $HCl_{(aq)}$ molecules in the droplet, then the number of $HCl_{(g)}$ molecules released increases linearly with the droplet volume (d_d^3). However, the number of $HNO_{3(g)}$ collisions increases linearly with droplet surface area (d_d^2). The net effect is the fraction of $HNO_{3(g)}$ collisions with the droplet surface that produce $HCl_{(g)}$ *increases* linearly with droplet diameter. This concept is illustrated in Figure 8 where the reactive uptake coefficient ($\gamma_{o,net}$) is plotted vs droplet diameter. Since uptake onto larger droplet sizes was measured relative to 100 nm diameter droplets, the values of $\gamma_{o,net}$ are scaled to the absolute measurement at 100 nm. The reactive uptake coefficients obtained in this work are consistent with the uptake coefficient measured by Abbatt and Waschewsky of ≥ 0.2 for a droplet size distribution spanning 1−5 μm in diameter.[13] Above about 2 μm in diameter, uptake will become limited by the rate of $HNO_{3(g)}$ diffusion to the droplet surface, and the mole fraction of chloride remaining in the droplet will begin to increase with increasing droplet size. This prediction is consistent with recent ambient sea-salt measurements. Yao et al.[60] found that as the particle size increased from ca. 0.8 to 10 μm the depletion of chloride in sea-salt aerosols decreased. Likewise, Wall et al.[61] observed increasing chloride depletion for smaller particles within the coarse size mode (>1.8 μm diameter).

It should be noted that the results presented here are inconsistent with Guimbaud et al. [14] who report a reactive uptake coefficient of 0.5 ± 0.2 for supersaturated (55% RH) 70 nm

diameter sea-salt droplets (P_{HNO_3} < 100 ppb). The reason for this discrepancy is not clear, although the droplet chemical compositions are different in the two experiments. (The higher chloride concentration in supersaturated droplets will give larger reaction rates and uptake coefficients—see eq 5.) The results of Davies and Cox[10] suggest that at relative humidities and nitric acid pressures comparable to the ones studied here the uptake coefficient will be on the order of 1×10^{-2}, which is in agreement with our measurements (Figure 8). Their model also predicts higher uptake coefficients (>0.1) at the lower nitric acid concentrations of Guimbaud et al. Guimbaud et al. do report a decrease in the reaction rate for P_{HNO_3} > 100 ppb, yielding uptake coefficients closer to those measured here. Perhaps the discrepancy between our results and those of others at low nitric acid pressures is related to Figure 5. Our analysis assumed a linear relationship between the reaction rate constant and nitric acid concentration. However, the plot in Figure 5 does suggest some nonlinearity and perhaps a weaker dependence of the reaction rate constant with nitric acid concentration below 0.02 M (100 ppb). More work is needed to accurately assess the effects of higher initial chloride concentration (e.g., lower RH) and lower nitric acid concentration on the reaction rate and their implications for the reaction mechanism under these conditions.

Acknowledgment. This research was supported by the National Science Foundation under grant number CHE-0098831. The authors thank T. Baer and D. Worsnop for helpful discussions, and B. Finlayson-Pitts for sharing pre-publication results.

References and Notes

(1) Keene, W. C.; Sander, R.; Pszenny, A. A. P.; Vogt, R.; Crutzen, P. J.; Galloway, J. N. *J. Aerosol Sci.* **1998**, *29*, 339−356.
(2) Finlayson-Pitts, B. J.; Hemminger, J. C. *J. Phys. Chem. A* **2000**, *104*, 11463−11477.
(3) Paerl, H. W. *Environ. Sci. Technol.* **2002**, *36*, 323A−326A.
(4) Murphy, D. M.; Anderson, J. R.; Quinn, P. K.; McInnes, L. M.; Brectel, F. J.; Kreindenweis, S. M.; Middlebrook, A. M.; Posfal, M.; Thomson, D. S.; Buseck, P. R. *Nature* **1998**, *392*.
(5) Rosenfeld, D.; Lahav, R.; Khain, A.; Pinsky, M. *Science* **2002**, *297*, 1667−1670.
(6) Ellison, G. B.; Tuck, A. F.; Vaida, V. *J. Geophys. Res.* **1999**, *104*, 11633−11642.
(7) Middlebrook, A. M.; Murphy, D. M.; Thomson, D. S. *J. Geophys. Res.* **1998**, *103*, 16475−16483.
(8) Beichert, P.; Finalyson-Pitts, B. J. *J. Phys. Chem.* **1996**, *100*, 15218−15228.
(9) Fenter, F. F.; Caloz, F.; Rossi, M. J. *J. Phys. Chem.* **1994**, *98*, 9801−9810.
(10) Davies, J. A.; Cox, R. A. *J. Phys. Chem. A* **1998**, *102*, 7631−7642.
(11) Leu, M.-T.; Timonen, R. S.; Keyser, L. F.; Yung, Y. L. *J. Phys. Chem.* **1995**, *99*, 13203−13212.
(12) ten Brink, H. M. *J. Aerosol Sci.* **1998**, *29*, 57−64.
(13) Abbatt, J. P. D.; Waschewsky, G. C. G. *J. Phys. Chem. A* **1998**, *102*, 3719−3725.
(14) Guimbaud, C.; Arens, F.; Gutzwiller, L.; Gaggeler, H. W.; Ammann, M. *Atmos. Chem. Phys.* **2002**, *2*, 249−257.
(15) Ghosal, S.; Hemminger, J. C. *J. Phys. Chem. A* **1999**, *103*, 4777−4781.
(16) Allen, H. C.; Laux, J. M.; Vogt, R.; Finalyson-Pitts, B. J.; Hemminger, J. C. *J. Phys. Chem.* **1996**, *100*, 6371−6375.
(17) Johnston, M. V. *J. Mass Spectrom.* **2000**, *35*, 585−595.
(18) Noble, C. A.; Prather, K. A. *Mass Spectrom. Rev.* **2000**, *19*, 248−274.
(19) Gard, E.; Kleeman, M. J.; Gross, D. S.; Hughes, L. S.; Allen, J. O.; Morrical, B. D.; Fergenson, D. P.; Dienes, T.; Galli, M. E.; Johnson, R. J.; Cass, G. R.; Prather, K. A. *Science* **1998**, *279*, 1184−1187.
(20) Carson, P. G.; Johnston, M. V.; Wexler, A. S. *Aerosol Sci. Technol.* **1997**, *26*, 291−300.
(21) Mansoori, B. A.; Johnston, M. V.; Wexler, A. S. *Anal. Chem.* **1994**, *66*, 3681−3687.
(22) Ge, Z.; Wexler, A. S.; Johnston, M. V. *J. Phys. Chem. A* **1998**, *102*, 173−180.
(23) Guazzotti, S. A.; Whiteaker, J. R.; Suess, D.; Coffee, K. R.; Prather, K. A. *Atmos. Environ.* **2001**, *35*, 3229−3240.
(24) Fergenson, D. P.; Song, X. H.; Ramadan, Z.; Allen, J. O.; Hughes, L. S.; Cass, G. R.; Hopke, P. K.; Prather, K. A. *Anal. Chem.* **2001**, *73*, 3535−3541.
(25) Winer, A. M.; Peters, J. W.; Smith, J. P.; Pitts, J. N. J. *Environ. Sci. Technol.* **1974**, *8*, 1118−1121.
(26) Yamamoto, M.; Tamaki, M.; Bandow, H.; Maeda, Y. *Atmos. Environ.* **2001**, *35*, 5339−5346.
(27) Cruz, C. N.; Pandis, S. N. *Atmos. Environ.* **1997**, *31*, 2205−2214.
(28) Cruz, C. N.; Pandis, S. N. *J. Geophys. Res.* **1998**, *103* (13), 111−113, 123.
(29) Cruz, C. N.; Pandis, S. N. *Aerosol Sci. Technol.* **1999**, *31*, 392−407.
(30) Cruz, C. N.; Dassios, K. G.; Pandis, S. N. *Atmos. Environ.* **2000**, *34*, 3897−3905.
(31) Cruz, C. N.; Pandis, S. N. *Environ. Sci. Technol.* **2000**, *34*, 4313−4319.
(32) Kane, S. M.; Leu, M.-T. *J. Phys. Chem. A* **2001**, *105*, 1411−1415.
(33) Cohen, M. D.; Flagan, R. C.; Seinfeld, J. H. *J. Phys. Chem.* **1987**, *91*, 4563−4574.
(34) Zhang, S.-H.; Akutus, Y.; Russell, L.; Flagan, R. C. *Aerosol Sci. Technol.* **1995**, *23*, 357−372.
(35) Kane, D. B.; Johnston, M. V. *Environ. Sci. Technol.* **2000**, *34*, 4887−4893.
(36) Liu, B. Y. H.; Ziemann, P. J.; Kittleson, D. B.; McMurry, P. H. *Aerosol Sci. Technol.* **1995**, *22*, 314−324.
(37) Kane, D. B.; Wang, J. J.; Frost, K.; Johnston, M. V. *Anal. Chem.* **2002**, *74*, 2092−2096.
(38) Neubauer, K. R.; Johnston, M. V.; Wexler, A. S. *Int. J. Mass Spectrom. Ion Processes* **1997**, *163*, 29−37.
(39) Mansoori, B. A.; Johnston, M. V.; Wexler, A. S. *Anal. Chim. Acta* **1998**, *359*, 185−191.
(40) Neubauer, K. R.; Johnston, M. V.; Wexler, A. S. *Atmos. Environ.* **1998**, *32*, 2521−2529.
(41) Jayne, J. T.; Worsnop, D. R.; Kolb, C. E.; Swartz, E.; Davidovits, P. *J. Phys. Chem.* **1996**, *100*, 8015−8022.
(42) Jayne, J. T.; Duan, S. X.; Davidovits, P.; Worsnop, D. R.; Zahniser, M. S.; Kolb, C. E. *J. Phys. Chem.* **1992**, *96*, 5452−5460.
(43) Swartz, E.; Shi, Q.; Davidovitz, P.; Jayne, J. T.; Worsnop, D. R.; Kolb, C. E. *J. Phys. Chem. A* **1999**, *103*, 8824−8833.
(44) Shi, Q.; Davidovitz, P.; Jayne, J. T.; Worsnop, D. R.; Kolb, C. E. *J. Phys. Chem. A* **1999**, *103*, 8812−8823.
(45) Finlayson-Pitts, B. J.; Pitts, J. N., Jr. *Atmospheric Chemistry: Fundamentals and Experimental Techniques*; John Wiley and Sons: New York, 1986.
(46) Donahue, N. M.; Clarke, J. S.; Demerjian, K. L.; Anderson, J. G. *J. Phys. Chem.* **1996**, *100*, 5821−5838.
(47) Worsnop, D. R.; Shi, Q.; Jayne, J. T.; Kolb, C. E.; Swartz, E.; Davidovits, P. *J. Aerosol Sci.* **2001**, *32*, 877−891.
(48) Li, Y. Q.; Davidovits, P.; Shi, Q.; Jayne, J. T.; Kolb, C. E.; Worsnop, D. R. *J. Phys. Chem. A* **2001**, *105*, 10627−10634.
(49) de Bruyn, W. J.; Shorter, J. A.; Davidovits, P.; Worsnop, D. R.; Zahniser, M. S.; Kolb, C. E. *Environ. Sci. Technol.* **1995**, *29*, 1179−1185.
(50) Worsnop, D. R.; Zahniser, M. S.; Kolb, C. E.; Gardner, J. A.; Watson, L. R.; Doren, J. M. V.; Jayne, J. T.; Davidovits, P. *J. Phys. Chem.* **1989**, *93*, 1159−1172.
(51) Jayne, J. T.; Leard, D. C.; Zhang, X.; Davidovits, P.; Smith, K. A.; Kolb, C. E.; Worsnop, D. R. *Aerosol Sci. Technol.* **2000**, *33*, 49−70.
(52) van Doren, J. M.; Watson, L. R.; Davidovits, P.; Worsnop, D. R.; Zahniser, M. S.; Kolb, C. E. *J. Phys. Chem.* **1990**, *94*, 3265−3269.
(53) Kolb, C. E.; Davidovits, P.; Jayne, J. T.; Shi, Q.; Worsnop, D. R. *Prog. React. Kinet. Mechanism* **2002**, *27*, 1−46.
(54) Smith, G. D.; Woods, E.; DeForest, C. L.; Baer, T.; Miller, R. E. *J. Phys. Chem. A* **2002**, *106*, 8085−8095.
(55) Morris, J. W.; Davidovits, P.; Jayne, J. T.; Jimenez, J. L.; Shi, Q.; Kolb, C. E.; Worsnop, D. R.; Barney, W. S.; Cass, G. R. *Geophys. Res. Lett.* **2002**, *29*, 1−4.
(56) Shi, B.; Seinfeld, J. H. *Atmos. Environ.* **1991**, *25A*, 2371−2383.
(57) Kumar, S. *Atmos. Environ.* **1989**, *23*, 2299−2304.
(58) Morris, J. R.; Behr, P.; Antman, M. D.; Ringeisen, B. R.; Splan, J.; Nathanson, G. *J. Phys. Chem. A* **2000**, *104*, 6738−6751.
(59) Pliego, J. R.; Riveros, J. M. *J. Phys. Chem. A* **2002**, *106*, 7434−7439.
(60) Yao, X.; Fang, M.; Chan, C. K. *Atmos. Environ.* **2003**, *37*, 743−751.
(61) Wall, S. M.; John, W.; Ondo, J. L. *Atmos. Environ.* **1988**, *22*, 1649−1656.